Spin-Orbit-Parity-Coupled Superconductivity in Topological Monolayer WTe_2

Ying-Ming Xie,[†] Benjamin T. Zhou,[†] and K. T. Law[*]
Department of Physics, Hong Kong University of Science and Technology, Clear Water Bay, 999077 Hong Kong, China

(Received 20 May 2020; accepted 11 August 2020; published 3 September 2020)

Recent experiments reported gate-induced superconductivity in the monolayer 1T′-WTe_2 which is a two-dimensional topological insulator in its normal state. The in-plane upper critical field B_{c2} is found to exceed the conventional Pauli paramagnetic limit B_p by one to three times. The enhancement cannot be explained by conventional spin-orbit coupling which vanishes due to inversion symmetry. In this Letter, we unveil some distinctive superconducting properties of centrosymmetric 1T′-WTe_2 which arise from the coupling of spin, momentum and band parity degrees of freedom. As a result of this spin-orbit-parity coupling (SOPC): (i) there is a first-order superconductor-metal transition at B_{c2} that is much higher than the Pauli paramagnetic limit B_p, (ii) spin-susceptibility is anisotropic with respect to in-plane directions and can result in possible anisotropic B_{c2}, and (iii) the B_{c2} exhibits a strong gate dependence as the spin-orbit-parity coupling is significant only near the topological band crossing points. The importance of SOPC on the topologically nontrivial inter-orbital pairing phase is also discussed. Our theory generally applies to centrosymmetric materials with topological band inversions.

DOI: 10.1103/PhysRevLett.125.107001

Introduction.—Recently, centrosymmetric monolayer 1T′-structure WTe_2, which is a two-dimensional topological insulator with helical edge states [1–5], has been found to become superconducting upon electrogating [6,7]. The coexistence of helical edge states and superconductivity establishes the system as a promising platform to create Majorana fermions [8,9] and thus attracts wide on-going attention. Interestingly, the in-plane B_{c2} of the superconducting topological insulator was found to be one to three times higher than the usual Pauli paramagnetic limit B_p [6,7].

It has been well established that spin-orbit couplings that lift spin degeneracies in electronic bands can enhance the B_{c2} in noncentrosymmetric superconductors [10,11]. In particular, Ising superconductors, such as noncentrosymmetric 2H-structured MoS_2, $NbSe_2$, and WS_2, have been shown to exhibit in-plane B_{c2} that is several times higher than B_p due to Ising spin-orbit coupling [12–23]. Despite similar chemical compositions and layered structures, 1T′-structured WTe_2 respects inversion symmetry such that spin-orbit coupling terms that involve only spin and momentum degrees of freedom are forbidden [1–3]. Therefore, the mechanism behind the observed enhancement of B_{c2} remains unknown.

In this Letter, we show that inversion symmetry allows the spin, momentum, and parities of the electronic states to couple in 1T′-WTe_2. We refer to this coupling as spin-orbit-parity coupling (SOPC). The SOPC not only opens a topological gap (as depicted in Fig. 1), and creates the helical edge modes [1–5], but it also pins the electron spins and renormalizes the effect of external Zeeman fields to enhance the B_{c2}. Importantly, the SOPC dramatically affects the superconducting properties such that (i) 1T′-WTe_2 undergoes a first-order superconductor-metal transition at B_{c2}, similar to conventional s-wave superconductors [24]; however, the transition happens at a much higher field than B_p. (ii) The spin susceptibility and B_{c2} can be anisotropic with respect to in-plane magnetic field directions. (iii) The B_{c2} is strongly gate dependent as the SOPC is effective only for states near the topological

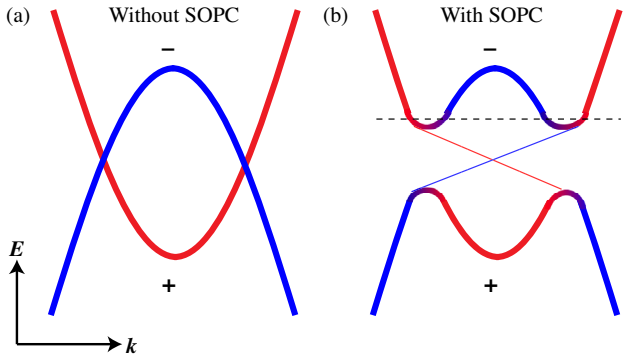

FIG. 1. Schematic band structure of two inverted bands without spin-orbit-parity coupling (SOPC) (a) and with SOPC coupling (b). The $+(-)$ sign labels the even (odd) parity of the band. Bands with even and odd parities in 1T′-WTe_2 originate predominantly from the d- and p-atomic orbitals, respectively. In (b), the SOPC opens a topologically nontrivial gap at the band crossing points and edge states emerge (thin lines in the gap). Only states close to the crossing points with heavily mixed orbital parities can experience strong SOPC. The horizontal dashed line in (b) denotes the chemical potential at which superconductivity is observed in the experiment.

TABLE I. Comparison among centrosymmetric spin-orbit-parity-coupled (SOPC), Ising, and conventional superconductivity.

Type of superconductors	SOPC	Ising	Conventional
Pairing correlations	Singlet	Singlet-triplet mixing	Singlet
$\chi_s(T=0)$	Zero	Finite	Zero
In-plane B_{c2}	$> B_p$	$> B_p$	$= B_p$
B-driven superconductor-metal transition as $T \to 0$	First order	Continuous	First order
Directional dependence of in-plane B_{c2}/χ_s	Anisotropic	Isotropic	Isotropic

band crossing points (band crossing involving bands with opposite parities). These properties distinguish superconductors with SOPC from noncentrosymmetric and convensional s-wave superconductors. Comparison among superconductors with SOPC, Ising superconductors, and conventional s-wave superconductors is presented in Table I.

Importantly, SOPC widely exists in topological materials such as superconducting Cu-doped Bi_2Se_3 [25–28]. However, orbital depairing effects in three-dimensional materials overwhelm the Zeeman effect in the superconducting state. Moreover, superconductivity in Cu-doped Bi_2Se_3 sets in when the chemical potential lies high above the band crossing points where the SOPC effect is weak [29,30]. Therefore, atomically thin 1T′-WTe_2, being superconducting near the band crossing points as depicted in Fig. 1(b), provides an ideal platform to study spin-orbit-parity-coupled superconductivity. Interestingly, we further show that SOPC is important for stablizing the interorbital pairing phases which can be topologically nontrivial.

Moreover, an enhanced B_{c2} has been observed in centrosymmetric monolayer 1T′-$MoTe_2$ [31], which was attributed to Rashba spin-orbit coupling due to gate-induced inversion breaking. Our theory suggests that the B_{c2} enhancement in 1T′-$MoTe_2$ can be readily explained by the SOPC and inversion breaking is inessential.

Model Hamiltonian of superconducting monolayer 1T′-WTe_2.—The symmetry group of a monolayer 1T′-WTe_2 is generated by time reversal, one in-plane mirror symmetry, and spatial inversion. These symmetries dictate the form of a four-band $\boldsymbol{k}\cdot\boldsymbol{p}$ Hamiltonian which describes the normal state of WTe_2 [1,32]:

$$H_0(\boldsymbol{k}) = \epsilon_0(\boldsymbol{k}) + \mathcal{M}(\boldsymbol{k})s_z + vk_x s_y + A_x k_x s_x \sigma_y + A_y k_y s_x \sigma_x + A_z k_y s_x \sigma_z, \quad (1)$$

where $\epsilon_0(\boldsymbol{k}) = t_x^+ k_x^2 + t_y^+ k_y^2 + \frac{1}{2}t_x' k_y^4 + \frac{1}{2}t_y' k_y^4 - \mu$, $\mathcal{M}(\boldsymbol{k}) = -\delta + t_x^- k_x^2 + t_y^- k_y^2 - \frac{1}{2}t_x' k_x^4 - \frac{1}{2}t_y' k_y^4$. Here, the s matrices operate on the orbital degrees of freedom formed by (p, d) orbitals with opposite parities, and σ matrices act on the spin space. Notably, δ determines the order of the band at $\boldsymbol{k}=0$. When $\delta > 0$, there is a band inversion while the SOPC terms open a topologically nontrivial gap and the system become a topological insulator as schematically depicted in Fig. 1(b). Derivation of the symmetry allowed terms and the model parameters are given in the Supplemental Material [32]. In H_0, the energy dispersions of the bands are given by $\xi_\pm(\boldsymbol{k})$ [as shown in Fig. 2(a)], with each band being twofold degenerate due to both the spatial inversion and time-reversal symmetries.

We emphasize that the usual spin-orbit coupling terms which involve $\boldsymbol{k}$ and σ only are forbidden by inversion symmetry. However, it is possible to have an SOPC term $\hat{\boldsymbol{g}}\cdot\boldsymbol{\sigma}$, where $\hat{\boldsymbol{g}} = (A_y k_y, A_x k_x, A_z k_y) s_x$. Importantly, the SOPC term is proportional to s_x and $\langle\Psi(\boldsymbol{k})|\hat{\boldsymbol{g}}\cdot\boldsymbol{\sigma}|\Psi(\boldsymbol{k})\rangle$ is significant only for Ψ with strongly hybridized p and d orbitals. This happens only near the topological band crossing points as schematically depicted in Fig. 1(b). Interestingly, superconductivity in 1T′-WTe_2 was observed experimentally when conduction band states near the band crossing points at $\pm Q$ are filled [Fig. 2(a)] with charge density $n \sim 10^{13}$ cm^{-2} [6,7]. Thus, 1T′-WTe_2 is an ideal platform to study the effects of SOPC on superconductivity.

Assuming on site attractive interactions to be dominant, the intraorbital singlet-pairing phase is expected to be energetically favorable. In this case, the superconducting state under an in-plane magnetic field $\boldsymbol{B}$ can be described by the Bogoliubovde Gennes Hamiltonian:

$$H_{\mathrm{BdG}}(\boldsymbol{k}) = H_0(\boldsymbol{k})\eta_3 + \frac{1}{2}g_s u_B \boldsymbol{B}\cdot\boldsymbol{\sigma} + \Delta\eta_1, \quad (2)$$

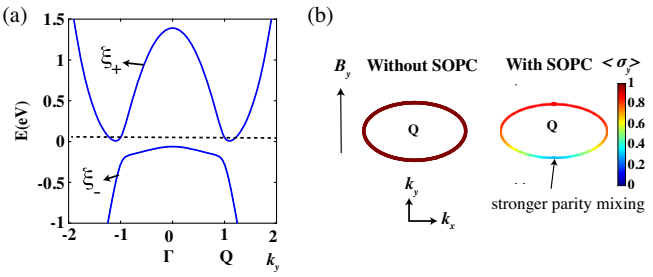

FIG. 2. (a) Normal-state band structure of monolayer WTe_2. Hybridyzation between p and d bands from SOPC opens a topologically nontrivial gap near $\pm Q$ and results in two Q valleys in the conduction bands. (b) Expectation value of spin-y component $\langle\sigma_y\rangle$ without (left) and with (right) SOPC on the Fermi surface contours under a weak Zeeman field $\boldsymbol{B} = B_y\hat{y}$ (Zeeman strength ~1 meV, contours around $+Q$ is shown here). The net spin along y direction induced by B_y is reduced by the pinning due to SOPC.

where η operates on particle-hole space, u_B is the Bohr magneton, $g_s = 2$ is the Land g factor.

To understand how SOPC affects the magnetic response to an external Zeeman field, it is instructive to project $H_{\mathrm{BdG}}(\boldsymbol{k})$ to a manifestly covariant pseudospin basis (MCPB) $\{|\boldsymbol{k},\alpha\rangle, |\boldsymbol{k},\beta\rangle\}$ [42–45] for the conduction band with energy $\xi_+(\boldsymbol{k})$, where superconducting pairing is formed. The transformation properties of the MCPB basis can be found in the Supplemental Material [32]. By projecting $H_{\mathrm{BdG}}(\boldsymbol{k})$ into the subspace $(\psi^\dagger_{\boldsymbol{k},\alpha}, \psi^\dagger_{\boldsymbol{k},\beta}, \psi_{-\boldsymbol{k},\beta}, -\psi_{-\boldsymbol{k},\alpha})$, the effective pairing Hamiltonian has the form:

$$H_{\mathrm{eff}}(\boldsymbol{k}) = \xi_{\boldsymbol{k}}\eta_3 + \frac{1}{2} g_s u_B \boldsymbol{B}\cdot\tilde{\boldsymbol{\sigma}}(\boldsymbol{k}) + \Delta\eta_1, \tag{3}$$

where $\tilde{\sigma}_i^{l,l'}(\boldsymbol{k}) = \langle \boldsymbol{k}, l|\sigma_i|\boldsymbol{k}, l'\rangle = \sum_j a_{ij}(\boldsymbol{k})\rho_j^{l,l'}$ (ρ_j: Pauli matrix in the pseudospin basis) is the projected spin operator in the pseudospin subspace, and the effect of SOPC on electron spins are encoded in the coefficients $a_{ij}(\boldsymbol{k})$ [see Supplemental Material [32] for explicit forms of $a_{ij}(\boldsymbol{k})$]. It is clear from Eq. (3) that the Zeeman effect due to external magnetic fields is renormalized by the SOPC term.

To demonstrate the renormalization and the spin-pinning effect encoded in $a_{ij}(\boldsymbol{k})$, we assume a weak Zeeman field $\boldsymbol{B} = B_y\hat{y}$ in H_{eff} and plot the Zeeman field induced spin expectation value in the y direction $\langle\sigma_y\rangle$ for states near the Q point with and without SOPC in Fig. 2(b). Evidently, without SOPC, spins along the Fermi surface contours can freely align with B_y. In contrast, in the presence of SOPC, spins at different $\boldsymbol{k}$ are pinned predominantly to the x direction as the $A_y k_y s_x \sigma_x$ term dominates [32]. It is important to note that, in Fig. 2(b), the spin pinning is much stronger for states with smaller k_y near the band crossing point due to the stronger mixing between p and d orbitals in these states. This clearly demonstrates the SOPC effect is not determined by the spin-orbit coupling part $A_y k_y \sigma_x$ alone, but also largely governed by the parity mixing operator s_x. In the next section, we show the important effects of SOPC on B_{c2}.

Enhancement, anisotropy, and gate dependence of in-plane B_{c2}.—Phenomenologically, the normal-state and superconducting free energy densities due to an external in-plane field $\boldsymbol{B}$ ($B = |\boldsymbol{B}|$) and pairing can be written as $f_n(B) = -\frac{1}{2}\chi_n B^2$, and $f_s(B) = f_{\mathrm{cond}} + f_{\mathrm{spin}}$ respectively. Here, χ_n and χ_s are the normal-state and superconducting spin susceptibilities, respectively, $f_{\mathrm{cond}} = -\frac{1}{2}N(E_F)\Delta_0^2$, with $\Delta_0 = \Delta(B = 0)$, is the zero-field condensation energy with $N(E_F)$ being the density of states at Fermi energy, and $f_{\mathrm{spin}} = -\frac{1}{2}\chi_s B^2$ is the spin magnetic energy in the superconducting state. B_{c2} can be estimated by identifying the point $f_n(B) = f_s(B)$, yielding $B_{c2} \approx B_p\sqrt{\chi_0/(\chi_n - \chi_s)}$, where $B_p = \Delta_0/(\sqrt{2}\mu_B)$, and $\chi_0 = 2N(E_F)u_B^2$ is the Pauli spin susceptibility of free electron gas. Clearly, B_{c2} can be enhanced to be higher than B_p via (i) a reduced $\chi_n < \chi_0$ and (ii) a residue $\chi_s \neq 0$. As shown in the MCPB basis, H_{eff} has the form of a spin-singlet superconductor, and we expect that the superconducting ground state cannot respond to a weak external Zeeman fields, which implies that $\chi_s = 0$ in the $T \to 0$ limit.

To demonstrate the vanishing χ_s in WTe_2, we calculate the superconducting spin susceptibility χ_s^{ii} ($i = x, y$) given by [46,47]:

$$\begin{aligned}\chi_s^{ii} &= -\frac{1}{2}u_B^2 k_B T\sum_{\boldsymbol{k},n}\mathrm{Tr}[\tilde{\sigma}_i\mathcal{G}(\boldsymbol{k}, i\omega_n)\tilde{\sigma}_i\mathcal{G}(\boldsymbol{k}, i\omega_n)] \\ &= \frac{1}{2}u_B^2\beta\sum_{\boldsymbol{k}}\gamma_i(\boldsymbol{k})\frac{1}{1+\cosh(\beta\sqrt{\xi_{\boldsymbol{k}}^2+\Delta^2})},\end{aligned} \tag{4}$$

where $\mathcal{G}(\boldsymbol{k}, i\omega_n) = (i\omega_n - \xi_{\boldsymbol{k}}\eta_3 - \Delta\eta_1)^{-1}$ is the Gor'kov Green's function obtained from $H_{\mathrm{eff}}(\boldsymbol{k})$ in Eq. (3) under zero magnetic field. T is the temperature, $\beta = 1/k_B T$, $\omega_n = (2n+1)\pi/k_B T$ denotes the fermionic Matsubara frequency. $\gamma_i(\boldsymbol{k}) = 2\sum_j a_{ij}^2(\boldsymbol{k})$ characterizes the renormalization effect on spins due to SOPC. Clearly, the denominator in the summand in Eq. (4) diverges as $T \to 0$ due to a finite superconducting gap Δ, thus $\chi_s^{ii}(T \to 0) = 0$ [Fig. 3(a)].

The vanishing χ_s^{ii} leaves us with the mechanism of enhanced B_{c2} via reduced χ_n. Note that χ_n is directly given by $\chi_s(\Delta = 0)$ in Eq. (5), i.e.,

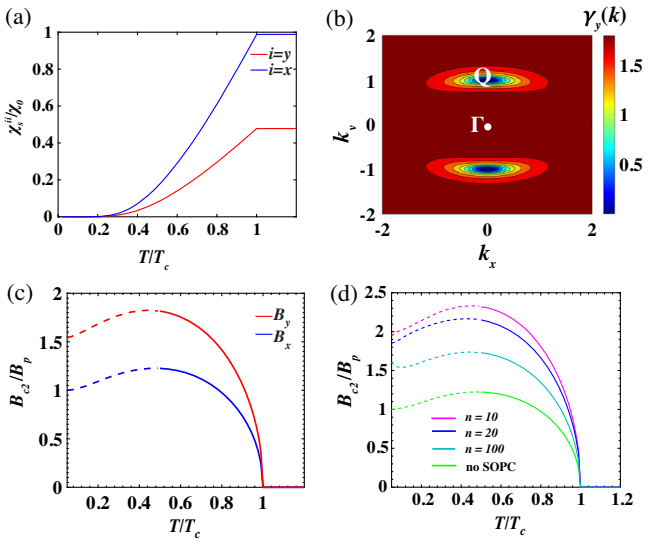

FIG. 3. Enhancement of B_{c2} via SOPC for 1T′-WTe_2. (a) Spin susceptibility χ_n^{ii} ($i = x, y$) as a function of temperature T, where the SOPC strength is $A_y = 0.855$ eV Å, Fermi energy $E_F = 100$ meV. We set $T_c = 1$ K according to experimental observations. (b) Value of γ_y at different $\boldsymbol{k}$. $\gamma_y(\boldsymbol{k})$ approaches zero near the band minimum at $\pm Q$. (c) $B_{c2} - T_c$ curves for $\boldsymbol{B} = B_x\hat{x}$ (blue) and $\boldsymbol{B} = B_y\hat{y}$ (red). Other parameters are the same as in (a). (d) $B_{c2} - T_c$ curves for $\boldsymbol{B} = B_y\hat{y}$ with different carrier density n in units of 10^{12} cm^{-2} and $A_y = 1.71$ eV Å. The case without SOPC (light green curve) is presented for reference.

$$\chi_n^{ii} = \frac{1}{2} u_B^2 \beta \sum_{\boldsymbol{k}} \frac{\gamma_i(\boldsymbol{k})}{1+\cosh(\beta\xi_{\boldsymbol{k}})} = u_B^2 N(E_F)\gamma_i(E_F), \quad (5)$$

where $\gamma_i(E_F) = \int d^2\boldsymbol{k}\gamma_i(\boldsymbol{k})\delta(\xi_{\boldsymbol{k}} - E_F)/\int d^2\boldsymbol{k}\delta(\xi_{\boldsymbol{k}} - E_F)$ is the averaged renormalization factor due to SOPC over the Fermi surface (see the Supplemental Material [32]).

As shown in Eq. (5), the normal-state spin susceptibility is given by $\chi_n^{ii} = \gamma_i(E_F)\chi_0/2$, with a renormalization factor $\gamma_i(E_F)/2$ due to SOPC. In the low temperature limit, the in-plane critical field along the i direction ($i = x,\ y$) is directly related to the Pauli limit by $B_{c2}^{ii} = B_p\sqrt{\chi_0/\chi_n^{ii}} = B_p\sqrt{2/\gamma_i(E_F)}$, which implies that $B_{c2} > B_p$ when $\gamma_i(E_F) < 2$.

To show the reduced χ_n^{yy}, we plot $\gamma_y(\boldsymbol{k})$ in the conduction band [Fig. 3(b)]. Evidently, $\gamma_y(\boldsymbol{k}) < 2$ holds throughout the whole Brillouin zone. As a result, $\gamma_y(E_F) < 2$ in general, leading to $\chi_n^{yy} < \chi_0$ as consistent with the result in Fig. 3(a, red curve) where $\chi_s^{yy} = \chi_n^{yy} < \chi_0$ for $T > T_c$.

In contrast, we noticed that $\chi_s^{xx} = \chi_n^{xx} \approx \chi_0$ for $T > T_c$ [blue curve in Fig. 3(a)]. This is because $\boldsymbol{B} = B_x\hat{x}$ is collinear with the dominant SOPC term $A_y k_y s_x \sigma_x$ and thus can freely align spins to the x direction. As a result, $B_{c2}^{yy} > B_p$ while $B_{c2}^{xx} \approx B_p$ as shown in the $B_{c2} - T_c$ curves in Fig. 3(c) obtained by solving the linearized gap equation:

$$\frac{2}{U/V} = k_B T \sum_{\boldsymbol{k},n} \mathrm{Tr}[G^{(0)}(\boldsymbol{k}, i\omega_n)\rho_y G^{(0)T}(-\boldsymbol{k}, -i\omega_n)\rho_y]. \quad (6)$$

Here, U is electron-phonon interaction strength, V is the sample volume, $G^{(0)}(\boldsymbol{k}, i\omega_n)$ is the normal state Green's function of $H_{\mathrm{eff}}(\boldsymbol{k})$ given in Eq. (3) (see the Supplemental Material [32] for details). Thus, our results suggest the B_{c2} of an SOPC superconductor can exhibit a strong anisotropy due to the anisotropic SOPC. This provides a distinctive signature of the possible SOPC origin behind the enhanced B_{c2} which is different from the isotropic B_{c2} and χ_s in both Ising superconductors and conventional superconductors as summarized in Table I.

Interestingly, $\gamma_y(\boldsymbol{k})$ has a strong $\boldsymbol{k}$ dependence [Fig. 3(b)] with the renormalization being strongest [signified by a strongly reduced value of $\gamma_y(\boldsymbol{k})$] near the band crossing points at $\pm Q$. As E_F increases upon gating, outer Fermi circles enclosing $\pm Q$ are accessed and $\gamma_y(\boldsymbol{k})$ approaches $\gamma_0 = 2$ for free electron gas. This again reflects the *parity-mixing* nature of SOPC: the spin pinning effect due to SOPC terms is strongest near the band crossing points at $\pm Q$ where the p and d orbitals are strongly mixed. As $\boldsymbol{k}$ deviates from $\pm Q$, the parity mixing becomes weaker and the spin pinning effect is suppressed. Such strong dependence of $\gamma_y(\boldsymbol{k})$ on Fermi level implies a strong gate dependence in B_{c2}^{yy}. This is explicitly demonstrated by solving the linearized gap equation at different values of carrier density n [Fig. 3(d)]. Consistently, as n increases, the enhancement of B_{c2} is reduced.

Notably, for superconductors with SOPC, the low temperature sectors of the $B_{c2} - T_c$ curves obtained by linearized gap equations (dashed segments in the range $0 < T < T_1 \approx 0.5T_c$) do not represent the true values of B_{c2} but the supercooling critical field instead [24]. As we discuss next, the superconductor-metal transition at B_{c2} in this regime is in fact first order in nature.

First-order phase transition at B_{c2} in low temperature regime.—To understand the nature of the phase transition at B_{c2} in the low temperature regime, we study how the free energy of a superconducting monolayer WTe_2 evolves under $\boldsymbol{B}$. Based on the full $H_{\mathrm{BdG}}(\boldsymbol{k})$ in Eq. (2), the free energy of the SOPC superconductor as a function of Δ can be obtained as [32,48]:

$$f_s = \frac{V|\Delta|^2}{U} - \frac{1}{\beta}\sum_{\boldsymbol{k},n} \ln(1 + e^{-\beta\epsilon_{\boldsymbol{k},n}}), \quad (7)$$

where $\epsilon_{\boldsymbol{k},n}$ are the quasiparticle energies of $H_{\mathrm{BdG}}(\boldsymbol{k})$. With fixed SOPC strength $A_y = 1.71$ eV Å and carrier density $n = 10 \times 10^{12}$ cm^{-2}, the evolution of $f_s - f_n$ at $T = 0.1T_c$ under increasing B is shown in Fig. 4(a) [note that $f_n \equiv f_s(\Delta = 0)$]. Clearly, for $0 < B < B_{c2}$, a local minimum in the free energy landscape develops at $\Delta = 0$ (purple curve) and eventually becomes the global minimum at $B = B_{c2}$ (red curve), where the superconductor-metal transition occurs. Notably, Δ drops abruptly to zero at B_c, which signifies a first-order phase transition.

The full self-consistent $B - T$ phase diagram from minimizing $f_s - f_n$ is shown in Fig. 4(b) with the phase boundary at B_{c2} accurately captured for all $T < T_c$. In accord with Fig. 4(a), the order parameter drops abruptly to zero at B_{c2} in the low temperature regime. We note that the mechanism of first-order transition in the low temperature limit for superconductors with SOPC is similar to a conventional superconductor, but the phase transition

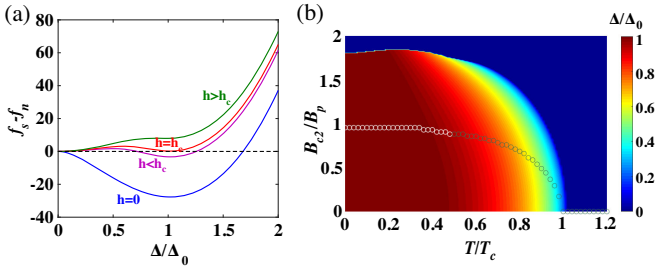

FIG. 4. (a) Landscapes of $f_s - f_n$ at $T = 0.1T_c$ in units of meV under $B = 0, 1.8B_p, 1.93B_p, 2.2B_p$. $B_{c2} \sim 1.93B_p$, with $\Delta_0 \approx 1.764k_BT_c$ at $B, T = 0$. (b) $B - T$ phase diagram from minimizing $f_s - f_n$ with $A_y = 1.71$ eV Å and $n = 10 \times 10^{12}$ cm^{-2}. The color represents the magnitude of Δ at different B and T. The line of circles represent the values of B_{c2} in a conventional superconductor, where $B_{c2}(T = 0) = B_p$. A first-order transition also occurs in the low temperature regime [24] (indicated by white circles).

happens much higher than B_p in SOPC superconductors as illustrated in Fig. 4(b). In particular, this distinctive first-order transition in the SOPC superconductor WTe_2 is very different from the continuous phase transition found in noncentrosymmetric Ising superconductors such as $NbSe_2$ due to a significant χ_s induced by Ising spin-orbit couplings [18,49,50].

Conclusion and discussions.—In this Letter, we identified a new class of centrosymmetric spin-orbit-parity-coupled superconductors where SOPC leads to enhancement of in-plane B_{c2} higher than B_p. In particular, we explained how the strong parity-mixing due to SOPC near the topologically nontrivial gap edge gives rise to a strongly enhanced B_{c2} in the superconducting topological monolayer WTe_2 with low electron carrier density. We further pointed out that the B_{c2} of SOPC superconductors can exhibit an anisotropy in in-plane field directions (but the anisotropy has not yet been observed experimentally). These properties are distinguished from both conventional superconductors and Ising superconductors as summarized in Table I.

While we considered an SOPC superconductor in the clean limit, we briefly discuss here the effect of disorder. By including potential fluctuation scattering and spin-orbit scattering effects in the Green function and the vertex correction to χ_s, we show that the B_{c2} is not sensitive to potential fluctuation scattering but a finite χ_s is induced by spin-orbit scattering, which further enhances the B_{c2} [32]. This explains why a higher $B_{c2} \approx 4B_p$ was observed in the more disordered sample [6].

In the main text, we assumed intraorbital pairing in Eq. (2) belonging to the A_g representation of the C_{2h} point group. Here, we discuss the effect of an interorbital singlet pairing: $\hat{\Delta}_1 = \Delta_1 \eta_1 s_x$, which belongs to the B_u representation of C_{2h}. First, we show that the B_u phase can be favored only when the band mixing due to SOPC is strong because significant contributions from both parity-odd and parity-even orbitals at the Fermi energy are needed for the pairing to be effective [32]. Interestingly, such an odd-parity pairing leads to a DIII class topological superconductor when the Fermi surface encloses odd number of time-reversal-invariant-momentum (TRIM) points [27]. In fact, projecting $\hat{\Delta}_1$ to the MCPB basis explicitly reveals that the combination of $\hat{\Delta}_1$ and SOPC results in an effective $p_x \pm ip_y$ pairing [32].

Unfortunately, superconductivity in monolayer WTe_2 sets in when the Fermi surface consists of two disconnected Q pockets away from the TRIM points (Fig. 2). Thus, the system remains topologically trivial. Only by artificially tuning the chemical potential to enclose the Γ point, helical Majorana modes can emerge on the edge [32]. Moreover, the effective p-wave pairing can result in large χ_s^{yy} and divergent B_{c2}^{yy}, which were not observed experimentally [6,7]. Thus, we believe that the B_u phase is less likely to be manifested experimentally in WTe_2.

The authors thank Wenyu He, Noah F. Q. Yuan for discussions and Mengli Hu and Junwei Liu for showing us the band structure of 1T′-WTe_2 from first-principle calculations. K. T. L. acknowledges the support of the Croucher Foundation and Hong Kong Research Grants Council (HKRGC) through Grants No. C6025-19G, No. C6026-16W, No. 16310219, and No. 16309718.

Note added.—After presenting the main findings of this work [51], we noticed that the enhancement of B_{c2} was observed in nontopological centrosymmetric materials without band inversion such as in few-layer stanene and ultrathin $PdTe_2$ [52–54]. The enhanced B_{c2} in these materials originates mainly from $\boldsymbol{k}$-independent atomic spin-orbital coupling, which is very different from the SOPC effect studied in this work.

*Corresponding author.
phlaw@ust.hk
†These authors contributed equally to this work.

[1] X. Qian, J. Liu, L. Fu, and J. Li, Science **346**, 1344 (2014).
[2] L. Muechler, A. Alexandradinata, T. Neupert, and R. Car, Phys. Rev. X **6**, 041069 (2016).
[3] S. Tang *et al.*, Nat. Phys. **13**, 683 (2017).
[4] Z. Fei, T. Palomaki, S. Wu, W. Zhao, X. Cai, B. Sun, P. Nguyen, J. Finney, X. Xu, and D. H. Cobden, Nat. Phys. **13**, 677 (2017).
[5] S. Wu, V. Fatemi, Q. D. Gibson, K. Watanabe, T. Taniguchi, R. J. Cava, and P. Jarillo-Herrero, Science **359**, 76 (2018).
[6] V. Fatemi, S. Wu, Y. Cao, L. Bretheau, Q. D. Gibson, K. Watanabe, T. Taniguchi, R. J. Cava, and P. Jarillo-Herrero, Science **362**, 926 (2018).
[7] E. Sajadi, T. Palomaki, Z. Fei, W. Zhao, P. Bement, C. Olsen, S. Luescher, X. Xu, J. A. Folk, and D. H. Cobden, Science **362**, 922 (2018).
[8] L. Fu and C. L. Kane, Phys. Rev. B **79**, 161408(R) (2009).
[9] J. Nilsson, A. R. Akhmerov, and C. W. J. Beenakker, Phys. Rev. Lett. **101**, 120403 (2008).
[10] P. A. Frigeri, D. F. Agterberg, A. Koga, and M. Sigrist, Phys. Rev. Lett. **92**, 097001 (2004).
[11] L. P. Gor'kov and E. I. Rashba, Phys. Rev. Lett. **87**, 037004 (2001).
[12] J. M. Lu, O. Zheliuk, I. Leermakers, N. F. Q. Yuan, U. Zeitler, K. T. Law, and J. T. Ye, Science **350**, 1353 (2015).
[13] X. Xi, Z. Wang, W. Zhao, J.-H. Park, K. T. Law, H. Berger, L. Forr, J. Shan, and K. F. Mak, Nat. Phys. **12**, 139 (2016).
[14] Y. Saito *et al.*, Nat. Phys. **12**, 144 (2016).
[15] S. C. de la Barrera, M. R. Sinko, D. P. Gopalan, N. Sivadas, K. L. Seyler, K. Watanabe, T. Taniguchi, A. W. Tsen, X. Xu, D. Xiao, and B. M. Hunt, Nat. Commun. **9**, 1427 (2018).
[16] J. Lu, O. Zheliuk, Q. Chen, I. Leermakers, N. E. Hussey, U. Zeitler, and J. Ye, Proc. Natl. Acad. Sci. U.S.A. **115**, 3551 (2018).
[17] Y. Xing, K. Zhao, P. Shan, F. Zheng, Y. Zhang, H. Fu, Y. Liu, M. Tian, C. Xi, H. Liu, J. Feng, X. Lin, S. Ji, X. Chen, Q.-K. Xue, and J. Wang, Nano Lett. **17**, 6802 (2017).

[18] E. Sohn, X. Xi, W.-Y. He, S. Jiang, Z. Wang, K. Kang, J.-H. Park, H. Berger, L. Forró, K. T. Law, J. Shan, and K. F. Mak, Nat. Mater. **17**, 504 (2018).

[19] B. T. Zhou, N. F. Q. Yuan, H.-L. Jiang, and K. T. Law, Phys. Rev. B **93**, 180501(R) (2016).

[20] W.-Y. He, B. T. Zhou, J. J. He, N. F. Q. Yuan, T. Zhang, and K. T. Law, Commun. Phys. **1**, 40 (2018).

[21] G. Sharma and S. Tewari, Phys. Rev. B **94**, 094515 (2016).

[22] S. Ilić, J. S. Meyer, and M. Houzet, Phys. Rev. Lett. **119**, 117001 (2017).

[23] J. Zhang and V. Aji, Phys. Rev. B **94**, 060501(R) (2016).

[24] K. Maki and T. Tsuneto, Prog. Theor. Phys. **31**, 945 (1964).

[25] H. Zhang, C.-X. Liu, X.-L. Qi, X. Dai, Z. Fang, and S.-C. Zhang, Nat. Phys. **5**, 438 (2009).

[26] C. X. Liu, X. L. Qi, H. J. Zhang, X. Dai, Z. Fang, and S.-C. Zhang, Phys. Rev. B **82**, 045122 (2010).

[27] L. Fu and E. Berg, Phys. Rev. Lett. **105**, 097001 (2010).

[28] T. Hashimoto, K. Yada, A. Yamakage, M. Sato, and Y. Tanaka, J. Phys. Soc. Jpn. **82**, 044704 (2013).

[29] Y. S. Hor, A. J. Williams, J. G. Checkelsky, P. Roushan, J. Seo, Q. Xu, H. W. Zandbergen, A. Yazdani, N. P. Ong, and R. J. Cava, Phys. Rev. Lett. **104**, 057001 (2010).

[30] L. A. Wray, S.-Y. Xu, Y. Xia, Y. S. Hor, D. Qian, A. V. Fedorov, H. Lin, A. Bansil, R. J. Cava, and M. Z. Hasan, Nat. Phys. **6**, 855 (2010).

[31] D. Rhodes, N. F. Yuan, Y. Jung, A. Antony, H. Wang, B. Kim, Y.-c. Chiu, T. Taniguchi, K. Watanabe, K. Barmak, L. Balicas, C. R. Dean, X. Qian, L. Fu, A. N. Pasupathy, and J. Hone, arXiv:1905.06508.

[32] See the Supplemental Material at http://link.aps.org/supplemental/10.1103/PhysRevLett.125.107001 for (i) $k \cdot p$ model of monolayer 1 T′-WTe_2, (ii) effective pairing Hamiltonian for SOPC superconductors, (iii) Pauli spin susceptibility and renormalization factor γ_i, (iv) B_{c2} from the linearized gap equation, (v) derivation of superconducting free energy, (vi) spin susceptibility with nonmagnetic impurity scattering, and (vii) discussions on possible inter-orbital pairing phases, which includes Refs. [33–41].

[33] X. Lin and J. Ni, Phys. Rev. B **95**, 245436 (2017).

[34] D.-H. Choe, H.-J. Sung, and K. J. Chang, Phys. Rev. B **93**, 125109 (2016).

[35] L.-K. Shi and J. C. W. Song, Phys. Rev. B **99**, 035403 (2019).

[36] R. A. Klemm, A. Luther, and M. R. Beasley, Phys. Rev. B **12**, 877 (1975).

[37] B. Dóra, A. Virosztek, and K. Maki, Phys. Rev. B **66**, 115112 (2002).

[38] A. V. Balatsky, I. Vekhter, and J.-X. Zhu, Rev. Mod. Phys. **78**, 373 (2006).

[39] A. Abrikosov and L. Gorkov, Sov. Phys. JETP **8**, 1090 (1959).

[40] M. Tinkham, *Superconductivity by M. Tinkham* (Gordon and Breach, New York, 1965).

[41] J. Alicea, Phys. Rev. B **81**, 125318 (2010).

[42] S.-K. Yip, Phys. Rev. B **87**, 104505 (2013).

[43] L. Fu, Phys. Rev. Lett. **115**, 026401 (2015).

[44] J. W. F. Venderbos, V. Kozii, and L. Fu, Phys. Rev. B **94**, 180504(R) (2016).

[45] S.-K. Yip, arXiv:1609.04152.

[46] P. A. Frigeri, D. F. Agterberg, and M. Sigrist, New J. Phys. **6**, 115 (2004).

[47] A. Abrikosov and L. Gorkov, Sov. Phys. JETP **15**, 752 (1962).

[48] A. Altland and B. D. Simons, *Condensed Matter Field Theory* (Cambridge University Press, Cambridge, England, 2010).

[49] R. Wakatsuki and K. T. Law, arXiv:1604.04898.

[50] Y. Xie, B. T. Zhou, T. K. Ng, and K. T. Law, Phys. Rev. Research **2**, 013026 (2020).

[51] Y. Xie, W. He, and K. T. Law, in *APS Meeting Abstracts* (2019), https://meetings.aps.org/Meeting/MAR19/Session/P09.5.

[52] C. Wang, B. Lian, X. Guo, J. Mao, Z. Zhang, D. Zhang, B.-L. Gu, Y. Xu, and W. Duan, Phys. Rev. Lett. **123**, 126402 (2019).

[53] J. Falson, Y. Xu, M. Liao, Y. Zang, K. Zhu, C. Wang, Z. Zhang, H. Liu, W. Duan, K. He, H. Liu, J. H. Smet, D. Zhang, and Q.-K. Xue, Science **367**, 1454 (2020).

[54] Y. Liu, Y. Xu, J. Sun, C. Liu, Y. Liu, C. Wang, Z. Zhang, K. Gu, Y. Tang, C. Ding, H. Liu, H. Yao, X. Lin, L.Wang, Q. Xue, and J.Wang, Nano Lett. **20**, 5728 (2020).